Longitudinal proteomic analysis of T cell differentiation in vivo reveals dynamic changes of the interactome

Christian M. Beusch[1,2]*, Abdelhameed S. Dawood[1,2]*, Ahmet Ozdilek, Sarah L. Welbourn, Alexandra Flegle, Sakshi Malik[2], Christina Niavi[2,5], Akil Akhtar[2], Carly Roman[2,5], Autumn A. Gavora[2,5], David E. Gordon[1,2,3 #], and Mohamed S. Abdel-Hakeem[1,2,3,4,5,6 #,$]

[1] Pathology Advance Translational Research Unit (PATRU), Department of Pathology and Laboratory Medicine,
[2] Emory Vaccine Center,
[3] Winship Cancer Institute,
Emory University School of Medicine, Atlanta, GA, USA
[4] Cancer Biology Graduate Program,
[5] Immunology and Molecular Pathology Graduate Program,
Emory University, Atlanta, GA, USA
[6] Faculty of Pharmacy, Cairo University

**Equal contribution, [#]Corresponding authors, [$]Lead contact*

Abstract

T cell differentiation has been extensively studied on the cellular, transcriptional, and epigenetic levels. However, proteomic profiling of T cell differentiation directly *ex-vivo* has not been performed, despite numerous studies demonstrating discrepancy between transcriptional and proteomic profiles of cells. Here, we present the first exhaustive longitudinal proteomic profiling of T cell differentiation *in vivo* using the well-characterized lymphocytic choriomeningitis virus (LCMV) mouse model. We performed *ex-vivo* protein abundance profiling of effector to memory differentiation (T_{EFF}/T_{MEM}) and early to late exhausted T cell (Tex) differentiation following LCMV infection with the acute Armstrong and chronic Clone-13 strains, respectively. Our results show dynamic alterations of the T cell proteome during differentiation that are either common or distinct for acute and chronic infection. Importantly, several proteins that are significantly abundant for a specific cell state were not previously highlighted by transcriptional profiling. Thus, our study provides a comprehensive resource for the proteome of *in vivo* T cell differentiation that could unravel novel protein interactions with potential therapeutic implications.

Introduction

T cells are the main arm of the adaptive immune system combating tumor cells and intracellular pathogens including viruses. In the context of acute infection, naive T cells are activated giving rise to effector cells (T_{EFF}) which upon clearing the pathogen differentiate into memory T cells (T_{MEM})[1]. This is accompanied by extensive changes in the phenotypic, transcriptional, and epigenetic profiles of T cells[2, 3, 4, 5]. For chronic infections and cancer, antigen persistence accompanied by chronic inflammation and a skewed cytokine milieu lead to alternative T cell differentiation through the "exhaustion" pathway[6]. Exhausted T cells (T_{EX}) exhibit hierarchical loss of functions, as well as unique phenotypic, transcriptional, and epigenetic profiles distinct from T_{EFF}/T_{MEM}[1, 6, 7, 8, 9, 10, 11]. However, the proteomic landscape of T cell differentiation directly *ex vivo* is understudied. While transcriptomics captures a momentary view of RNA expression and epigenetics shed light on gene regulation, they do not provide a direct measurement of proteins which represent the primary molecular machines and the functional components that drive biology within a cell. Additionally, numerous studies highlighted the limited correlation between RNA and protein levels, and the discordance between the half-lives of mRNA and their corresponding proteins, underscoring the fact that transcriptional profiling is not an ideal proxy for protein expression[12, 13].

Several studies have tackled proteomic profiling of immune cell activation *in vitro*, where they demonstrated the extensive remodeling of the proteome upon activation, and heterogeneous correlation between protein abundance and mRNA quantification, thus confirming results from other fields of biology on the discordance between the proteome and transcriptome. However, all these studies were performed *in vitro*, and were mainly focused on the early stages of T cell activation upon brief antigenic stimulation[14, 15, 16, 17, 18]. Similar efforts were made to profile the proteome of *in vitro* activated human T cells[19, 20, 21]. Other studies aimed at profiling the proteome of human immune cells, and again demonstrated that proteomic profiling highlighted proteins that were overlooked in transcriptomic data sets that have potential as immunotherapeutic targets[22, 23]. Thus, comprehensive longitudinal proteomic profiling of CD8 T cells in a well-established model is needed to dissect the interactome of T cell differentiation.

Here, we profiled the dynamics of proteomic interactions during the differentiation of T cells *in vivo* in the context of acute versus chronic infection with LCMV Armstrong and Clone-13 strains, respectively. Our comprehensive analysis of global protein abundance data demonstrates a strong alignment with well-established knowledge of T cell biology, including key canonical markers associated with different cell states. We also identify several proteins of interest associated with T cell exhaustion and T_{EFF}/T_{MEM} differentiation previously not directly associated with T cell differentiation. Collectively, our data provides proof for the validity of our proteomics approach and provides novel insights into the protein-driven mechanisms underlying T cell differentiation. We identify several proteins of potential roles in T cell differentiation that were not previously reported, and that merit future validation.

Results

Longitudinal proteomic profiling of antigen-specific CD8 T cells shows significant modulation of the proteome upon activation followed by moderate modulations during differentiation.

Extensive phenotypic, transcriptional, and epigenetic profiling of T cell differentiation has greatly benefited from using the well-characterized lymphocytic choriomeningitis virus (LCMV) mouse model. By comparing mice infected with the Clone 13 strain (LCMV-Cl13) causing chronic infection to mice infected with the Armstrong strain (LCMV-Arm) causing acute infection[2, 8, 10, 24, 25, 26, 27]. Here, we used high-resolution Mass Spectroscopy (MassSpec) to characterize the proteome of antigen-specific T cells longitudinally at the different stages of both acute and chronic infections. For this, we adoptively transferred congenically distinct transgenic CD8 T cells (P14 cells) expressing the T cell receptor (TCR) specific for the LCMV glycoprotein epitope 33-41, GP33, into two groups of congenically distinct recipient mice. One group of mice was infected with the chronic LCMV-Cl13 strain, while the other was infected with the acute LCMV-Arm strain, respectively generating exhausted T cells (T_{EX}) and effector/memory T cells (T_{EFF}/T_{MEM}). P14 cells were isolated and sorted across a time course experiment 8, 15, and 30 days post-infection (hereafter d8, d15, and d30), representing the early, intermediate, and late stages of infection, in four replicate experiments. Naïve P14 cells were also sorted to provide a benchmark for protein expression in naïve T cells (Fig.1A). The sampling times were chosen based on the extensive literature previously published about LCMV infection in mice[2, 8, 10, 24, 26]. At least 2.1×10^5 (median 1.13×10^6) antigen-specific CD8 T cells were sorted from the different samples at high purity (Supp. Fig.1C), and frozen pellets were banked. All samples were processed together and were analyzed using our in-house TimsTOF Pro 2 mass spectrometer (Bruker) in DIA mode and searched using the industry-standard Spectronaut software package, Biognosys (Fig.1A).

Our flow cytometry analyses validated the previously reported phenotype of T_{EX} and T_{EFF}/T_{MEM} at the various phases of infection, compared to naïve T cells. This included the significantly higher levels of expression (as measured by mean fluorescence intensity, MFI) of canonical exhaustion markers, such as PD-1, Tox, and CD39 (encoded by *Entpd1*) on CD8 T cells harvested from chronically C13-infected mice, compared to the significant upregulation of activation markers KLRG1, CX3CR1, and CD44 on T_{EFF}, as well as GzmB production. Whereas differentiation into T_{MEM} was accompanied by the upregulation of the expression of the alpha subunit of interleukin-7 (IL-7) receptor, IL7Rα (CD127). As previously reported [1, 7, 10, 24, 26], we observed that the majority of T_{EFF} (d8 p-inf. with LCMV-Arm) exhibited that the activated phenotype KLRG1$^+$PD1$^-$CD127$^-$, that shifted to the KLRG1^{lo}CD127$^+$ phenotype as the cells transitioned to the T_{MEM} phenotype (d15 and d30 p-inf. with LCMV-Arm) (Fig.1B,C,D, and Supp. Fig.1A,B, Supp. Fig.2F). In parallel, the majority of early-T_{EX} (d8 p-inf. with LCMV-Cl13) displayed the PD1$^+$CD127$^-$ with a significantly lower frequency of cells that are KLRG1$^+$. The frequency of KLRG1$^+$ cells progressively decreased during the intermediate and late exhaustion phases that are (d15 and d30 p-inf. With LCMV-Cl13), whereas the majority of antigen-specific CD8 T cells remained PD1$^+$CD127$^-$.

We successfully quantified more than 6,700 proteins across the entire dataset, which meets our expectations based on similar cell types we have analyzed (Supp. Fig.2A). Expression levels for proteins from four biological replicates showed strong correlation (Supp. Fig.2B). Most importantly, the abundance of individual proteins displayed a wider dynamic

range than that of mRNAs; where protein measurements spanned several orders of magnitude more than that spanned by transcriptional profiling of mRNAs from previously published data (Supp Fig 2C-E). This means that relative measurements of protein abundance using MassSpec in our dataset can measure proteins with very low abundance, including transcription factors not highly expressed by a specific T cell state such as Tox expression in T_{EFF}/T_{MEM}, with comparable accuracy to top-ranked proteins such as GAPDH and histone proteins.

We next sought to confirm the concordance between the expression levels of canonical markers of T cell differentiation as measured by flow cytometry (MFI) and the protein abundance of the same markers quantified by MassSpec. This comparison validated that the relative protein abundance quantified by MassSpec of the canonical markers of the different cell states recapitulates the expression patterns measured by flow cytometry (Fig.1D-E, and Supp. Fig.1F,G). This was true for markers associated with activation and effector phenotype including granzyme B, CD44, CX3CR1, and KLRG1, as well as exhaustion-associated markers, such as PD1, Tox, and Entpd1.

Globally, differentiation of naive CD8 T cells in the context of acute or chronic infection was accompanied by substantial changes in their proteomic profile that followed two distinct pathways, as reflected in the principal component analysis (PCA) (Fig.1E). This confirmed the unique differentiation path for T_{EX} as compared to the T_{EFF}/T_{MEM} proteomically that was previously shown phenotypically[25, 26], transcriptionally[10, 24], and epigenetically[2, 8]. Quantitatively, activation from the naive T cell state to either T_{EFF} or early-T_{EX} was accompanied by changes in ~1,000 proteins, which is significantly higher than the protein modulations occurring at further stages of differentiation. Importantly, these proteomic changes from the naïve state included significant downregulation of 337-401 proteins, confirming previous findings that the naïve state of T cells is actively maintained[20] (Fig.1F). Significant changes continued as the antigen-specific CD8 T cells transitioned from a Teff-dominated response at the early stage of infection (d8) towards a T_{MEM}-dominated response at the intermediate stage of acute infection (d15) (~200 proteins changing), and to a much lesser extent from intermediate to late stages (only 22 proteins). However, during chronic infection significant proteome modulation extended from the early-intermediate exhaustion transition to the intermediate-late exhaustion transition, with changes in the levels of 200 and 114 proteins, respectively.

Overall, the dynamic protein changes accompanying transitions between cell states in acute and chronic infections are in line with previously reported transcriptional and epigenetic studies[2, 8, 10, 24]. Major modulation of the T cell proteome occurs following activation and transition from the naïve state, with subsequent more limited modulations as the cell differentiates during the intermediate and late stages of infection.

Expression profiles of proteins defining T cell activation and differentiation in the context of acute LCMV-Arm infection.

Previous work has demonstrated key phenotypic, transcriptional, and epigenetic markers and pathways in the differentiation of naïve T cells into effector then into memory T cells[1, 2, 3, 4, 5, 10, 24, 25, 26]. Several studies of early T cell differentiation upon brief *in vitro* stimulation demonstrated extensive remodeling of the proteome upon activation, as well as a degree of discordance between proteomic and transcriptomic quantifications, allowing the elucidation of several novel insights into the biology of T cell activation, and the specific roles of various transcription factors, kinases, and environmental cues in shaping the T cells proteome[14, 16, 17, 18, 19, 21]. However, the elucidation of the full extent of *in vivo* dynamic changes of the proteome longitudinally during the

169 various stages of acute infection accompanied by the differentiation of naïve T cells into
170 T_{EFF}/T_{MEM} has not been studied. We analyzed the high-resolution MassSpec profiling of the
171 proteome of antigen-specific CD8 P14 T cells sorted on d8, d15, and d30 post-infection (p.inf.)
172 with acute LCMV-Arm. Our analyses revealed extensive changes of the T cell proteome upon
173 activation, where the protein abundance of 962 proteins was significantly changed as the cells
174 differentiated from naïve to T_{EFF}, compared to less changes as the CD8 T cells transitioned from
175 the effector to the memory state as only 204 proteins significantly changed their abundance
176 between d8 and d15 post-infection with acute LCMV-Arm. Very limited change was observed
177 between the intermediate (d15) and late (d30) time points, where only 23 proteins were
178 significantly different between these two time points (Supp Fig.3A). Comparing each of the
179 T_{EFF}/T_{MEM} cell states at the various phases of infection to the initial naïve state confirmed these
180 dynamics, where the change in abundance of 301 proteins remained stable at the various
181 T_{EFF}/T_{MEM} cell states compared to 538 proteins that only exhibited statistically significant
182 between naïve and d8-T_{EFF} (Supp Fig.3B). Additionally, as with the pairwise analyses between
183 the different time points, the significant changes in protein abundance when comparing all time
184 points to naïve T cells reflected modest changes post the activation phase, with 97 proteins that
185 exclusively changed abundance between d8 and d15, and only 50 proteins were exclusive
186 between d15 and d30 (Supp Fig.3B).
187 Unsupervised clustering of our protein abundance data for CD8 T cell differentiation
188 during acute infection showed dynamic changes of the T cell proteome (Fig.2A). Compared to
189 naïve T cells, ten protein modules were observed that followed distinct kinetics (Fig.2A-B).
190 Clusters 1 and 2 represented modules that showed consistent downregulation post-activation of
191 naïve CD8 T cells, where the abundance of these proteins remained lower than that of naïve T
192 cells in T_{EFF}/T_{MEM} starting at the earliest time point examined (d8 p.inf.) until the latest time point
193 (d30 p.inf.). Other modules exhibited temporary downregulation, e.g. cluster 3 that showed
194 lower abundance of its proteins at the early stage of infection (d8), but regained a level of
195 expression comparable to naïve T cells by d15. Conversely, cluster 4 showed slower kinetics of
196 change, where the proteins within this cluster exhibited changes in their abundance only at the
197 intermediate stage of infection (d8), and these changes persisted until d30. Cluster 5 despite
198 lower abundance of its proteins at the early stage of infection (d8), they exhibited similar or
199 slightly higher levels than naïve T cells. The remaining clusters generally showed an increase
200 in their relative abundance compared to naïve T cells with variable kinetics. Whereas cluster 6
201 and 7 showed higher abundance of its proteins at the early stage of infection (d8), but regained
202 a level of expression comparable to naïve T cells or slightly higher by d15, clusters 8, 9 and 10
203 showed persistently higher abundance throughout the time course examined, with low,
204 intermediate or high abundance, respectively, compared to naïve. Some biological processes
205 associated with representative clusters are represented in Fig.2C. Where proteins in cluster 6
206 that exclusively show higher abundance of its proteins at the early stage of infection (d8), were
207 associated with DNA replication, metabolic processes, and mitotic cell processes. On the other
208 hand, proteins in clusters 9 and 10, that showed higher abundance sustained until d30, were
209 associated with inflammatory responses, leukocyte activation, and cell migration, as well as
210 killing of cells and granzyme-mediated pathways (Fig.2C).
211 Pairwise analysis focusing on individual proteins showed significantly increased protein
212 abundance of the canonical markers associated with each state (Fig.2D-F). Comparing the T_{EFF}
213 proteome from the peak of the immune response (d8) to either the naive state or the d15
214 proteome accompanied by the T_{EFF}-to-T_{MEM} transition showed increased abundance of Ki67

(encoded by the *Mki67* gene), granzyme B (*GzmB*), and CX3CR1, whereas the abundance of TCF-1 (*Tcf7*) was significantly higher in naïve/T_{MEM}. For the T_{EFF}/naïve comparison, many other proteins were significantly more abundant in the activated and highly functional T_{EFF}, such as the functional proteins GzmA, gamma-interferon (IFNγ) and perforin, the activation marker CD44, as well as the transcription factors T-bet (*Tbx21*) and Zeb2. Additionally, several proteins that were not among the top differential mRNAs in the microarray are currently under investigation for their potential roles in T cell differentiation in the context of acute infection.

Analyzing the correlation between our protein abundance analysis and transcriptional analysis using microarray data from Doering et al.[24], showed that generally there was a correlation between the changes in protein abundance measured by proteomics and the changes in mRNA measured by microarray (Fig.2G-I). Similar to the previous analyses, activation and functional markers were highly enriched in d8-T_{EFF} compared to naïve cells or d15 (Fig.2G), whereas memory markers became more enriched as the cells transitioned to a more profile by d15 (Fig.2H). Again, minimal changes were observed between d15 and d30 (Fig.2I).

Together, our longitudinal proteomic profiling of the protein abundance landscape of antigen-specific CD8 T cells during acute viral infection corroborated with transcriptional and epigenetic profiling of these cells, where extensive modulation occurs at the early stages of infection as the cell exits the naïve quiescent state into the activated antigen-experienced state, followed by moderate changes as they differentiate from the effector to the memory state. Our results also confirmed previous findings from proteomic profiling of eukaryotic cells that showed subtle differences in protein abundance of specific proteins as compared to the quantification of their corresponding mRNAs measured by transcriptional profiling. Several proteins revealed by our protein abundance were not previously investigated for their role in T cell differentiation in the context of acute infection and are under investigation.

Common and distinct dynamic changes of the T cell proteome in the context of acute LCMV-Arm and chronic LCMV-Cl13 infections.

T cell exhaustion is a hallmark of cancer and chronic viral infection. The generation of exhausted CD8 T cells (T_{EX}) is associated with failure to clear tumor cells and virus-infected cells, mainly due to progressive hierarchical loss of functions[6, 26, 27]. T cell exhaustion represents an independent differentiation path adopted by T_{EX} completely distinct from the differentiation path of effector/memory T cells (T_{EFF}/T_{MEM}) generated during acute infection[2, 9, 10, 26, 28, 29, 30]. This is reflected by the unique phenotypic, metabolic, transcriptional, and epigenetic profiles distinct from T_{EFF}/T_{MEM} that start very early post-infection[24, 31, 32,33, 34, 35, 36].

We harnessed the full potential of the LCMV mouse model that enables comparison of antigen-specific CD8 T cells with the same specificity during acute and chronic infection in parallel, and was the well-established model used to establish the uniqueness of phenotypic, metabolic, transcriptional, and epigenetic profiles of T_{EX} that start very early post-infection[24, 31, 32,33, 34, 35, 36]. Dissecting the protein abundance profile of P14 cells at the different stages of infection under both acute and chronic conditions compared to naive P14 cells revealed interesting dynamics of the proteome. The kinetics of protein abundance could be grouped into 16 modules (Fig3A, B). Some of these modules had comparable kinetics in both acute and chronic conditions, such as modules associated with exiting the naïve state, e.g. upregulated clusters C15/C16 and downregulated cluster C1/C2, that maintained the increased/decreased abundance compared to naïve throughout the course of infection. Other modules with common kinetics were associated with activation, where the protein abundance was significantly changed

262 at the early time point (d8) but reverted close to the naïve levels by d30 e.g. upregulated C9 and
263 downregulated cluster C5/C6. Some clusters showed gradual decrease/increase under both
264 settings, e.g. upregulated C11 and downregulated cluster C3.
265 Several biological processes were associated with the different proteomic modules that
266 are commonly regulated in CD8 T cells under both acute and chronic conditions (Supp. Fig.4B).
267 In the modules associated with exiting the naïve state, clusters containing proteins with higher
268 abundance compared to naïve cells (C15/C16) were associated with cytokine production,
269 inflammatory response, as well as leukocyte differentiation and migration, whereas lower
270 abundance clusters' proteins (C1/C2) were associated with processes such as negative
271 regulation of growth. Activation-specific clusters were associated with higher abundance of
272 proteins involved in pyrimidine nucleoside biosynthesis (C9), and lower abundance of proteins
273 associated with small molecule and lipid catabolism and galactose metabolism (C5/C6).
274 Thus, by profiling the protein abundance landscape of CD8 T cells using acute LCMV-
275 Arm in parallel with LCMV-Cl13 enabled defining common proteomic modules that suggests
276 they represent core program of T cell differentiation, compared to acute-specific and chronic-
277 specific programs (Fig.3A-B, and D-F).
278
279 **Specific proteomic modules are associated with T cell exhaustion during chronic LCMV-**
280 **Cl13 infection.**
281 Therapeutically targeting T_{EX} to reverse their dysfunction revolutionized cancer immunotherapy.
282 Immune checkpoint blockade (ICB) strategies, such as PD1:PDL1 pathway blockade, to
283 reinvigorate T_{EX} demonstrated significant success in curing cancer patients[37]. However, not all
284 patients benefit from immunotherapy[38], and ICB does not have the same success rate in all cancer
285 indications. Even successful checkpoint blockade is not durable in all cases due to lack of
286 modulation of the epigenetic landscape of T_{EX} by immunotherapy[8, 9] or upon complete cure of
287 chronic disease[39, 40]. Hence, there is an urgent need to further our mechanistic understanding of
288 T cell exhaustion, to rationally design novel therapeutic strategies that would expand the benefits
289 of immunotherapy to more patients and new indications.
290 Thus, we next focused our analyses on the exhaustion-specific modules (Fig.3A-C, and
291 Supp. Fig.4A-B) and pairwise comparison of T_{EX} versus T_{MEM} (Fig.3D-H, and Supp. Fig.4C-E),
292 especially during later stages of infection. Several modules within our unsupervised clustering
293 had distinct dynamics in T_{EX} compared to T_{EFF}/T_{MEM}. For some of these modules, there was
294 consistently relative higher abundance of component proteins in T_{EX} versus T_{EFF}/T_{MEM},
295 C4/C7/C10, whereas for other modules T_{EX} had differential kinetics compared to T_{EFF}/T_{MEM}, e.g.
296 C8/C12/C13/C14. GoTerm analysis of biological processes associated with the proteins leading
297 these modules revealed that clusters containing proteins with consistently higher abundance in
298 T_{EX} (C4/C7/C10) were associated with processes such as response to interferon-beta, negative
299 regulation of the immune system, and negative regulation of metabolic processes such as
300 proteolysis, peptidase activity, and hydrolase activity (Fig.3A-B, and Supp. Fig.4B). Clusters
301 with differential kinetics, where abundance of proteins in T_{EX} at the early stage of infection (d8)
302 was comparable to T_{EFF} but was higher than T_{MEM} at intermediate and late stages,
303 C12/C13/C14, were linked to lymphocyte activation, adaptive immune response, DNA
304 replication, and mitotic cell-cycle processes. Whereas the cluster that had higher protein
305 abundance in T_{EX} than T_{EFF} at the early stage of infection (d8) but lower abundance than T_{MEM} at
306 the late stage of infection (d30), C8, associated with translation, as well as peptide metabolism
307 and biosynthesis. Some of these biological processes showed extensive modulation of most of
308 their components in T_{EX} versus T_{EFF}/T_{MEM}, such as respiratory chain complex 1 and

309 mitochondrial ribosomes (Fig.3C, and Supp. Fig.4E), underscoring the significant impact of
310 proteome modulation on the flexibility of the cellular metabolic state.
311 A main advantage of using the LCMV-Arm in parallel with LCMV-Cl13 is the ability to
312 determine the core program of T cell differentiation versus acute-specific and chronic-specific
313 programs. Proteins associated with the core T cell differentiation program are reflected by the
314 intersection between Arm and Cl13 Venn diagrams, as well as proteins within the top-right and
315 bottom-left quadrants of the correlation graphs when compared to naïve proteomic profile
316 (Fig.3D-F). Pairwise analyses of the acute/Arm versus chronic/Cl13 protein abundance profiles
317 revealed proteins that are specific for each state at the different stages of infection, where 245,
318 351, and 292 proteins were significantly different between acute and chronic at the early,
319 intermediate, and late stages of infection, respectively (Supp. Fig.4A). Volcano plots highlighted
320 the T_{EX}-specific proteins of significant abundance compared to T_{EFF}/T_{MEM}, at the various stages
321 of infection (Fig.3G, and Supp. Fig.4C-D). Dissecting the proteomic profile of late-T_{EX} compared
322 to T_{MEM} by comparing LCMV-Cl13 and LCMV-Arm at d30 (Fig.3G) demonstrated significantly
323 elevated protein abundance of canonical exhaustion markers for late-T_{EX} that have been
324 extensively studied (red dots in the volcano plots). These included the inhibitory receptors
325 (IRs), CD39 (encoded by *Entpd1*), PD1 (*Pdcd1*), TIM3 (*Havcr2*), 2B4 (*Cd244*), LAG3 and TIGIT,
326 in addition to the transcription factors (TFs), Tox and Eomes. Additionally, proteins belonging to
327 the interferon-stimulated genes (ISGs) Isg15, Ifit1, and Isg20, several members of the granzyme
328 family granzyme-B, -K, and -A, the apoptosis-associated protein Caspase-3, and the
329 proliferation marker Ki67 (*Mki67*), were significantly more abundant in T_{EX}, as previously
330 reported. Some of these markers showed consistent higher protein abundance by T_{EX} versus
331 T_{EFF}/T_{MEM} at the various stages of chronic disease, including the hallmark marker of exhaustion
332 PD1, and other checkpoints such as LAG3 and TIGIT, as well as Tox, the main TF orchestrating
333 the exhaustion program[33, 34, 35] (Supp. Fig.4C-D). Conversely, the activation marker KLRG1
334 consistently exhibited lower abundance in T_{EX} versus T_{EFF}/T_{MEM}, in addition to lower abundance
335 of the memory-associated marker CD127 (*Il7r*) and TF TCF1 (*Tcf7*) at the intermediate and late
336 stages. This was also associated with enrichment in previously published signatures of T_{EX} and
337 dysfunctional CD8 T cells (Fig.3H). Additionally, several proteins that have not been extensively
338 studied for their role in the T_{EX} biology showed significantly different abundance in T_{EX} versus
339 T_{EFF}/T_{MEM} (gray dots in the volcano plots), which merits further investigation.
340 Together, these analyses show similar patterns for protein abundance of T_{EX}-associated
341 established markers that go in line with previously reported transcriptional and epigenetic
342 profiling in the same LCMV mouse model, as well as in other T cell exhaustion/dysfunction
343 models and datasets. More importantly, our protein abundance profiling of T_{EX} revealed novel
344 proteins with potential role in the exhaustion biology that requires further investigation to
345 validate their specific function.
346
347 **Integration of proteomic-transcriptomic profiling data of T cell differentiation.**
348 Transcriptomic analysis has been pivotal to our understanding of T cell differentiation. However,
349 for some genes mRNA amounts are unable to predict protein amounts upon T cell activation *in*
350 *vitro* [20, 41, 42]. However, the correlation between transcript and protein abundance during T cell
351 differentiation *in vivo* has not been elucidated.
352 We sought to compare the correlation between the fold-change in protein abundance in
353 comparison to the fold-change in transcripts between T_{EX} and T_{EFF}/T_{MEM} at the different stages
354 of infection using microarray data from Doering et al.[24] (Fig.4A). Our analyses revealed a

355 correlation coefficient of 0.47-0.49 for the late and intermediate time points, and even a lower
356 correlation (0.28) for the early stage of infection, suggesting moderate to low correlation
357 between measurements of the transcriptional changes and protein abundance changes across
358 the different time point. This could be attributed partially to the higher median protein intensity
359 compared to the median microarray counts (Supp. Fig.5A). Additionally, when categorizing the
360 transcriptional data according to the median transcript counts, it revealed that the main
361 discrepancy was for mRNAs with lower median counts (Fig.4B, and Supp. Fig.5B). This argues
362 for higher accuracy for protein abundance measurements over a wider dynamic range
363 compared to transcriptional measurements. However, when focusing on a specific group of
364 exhaustion-specific markers that were consistently higher in T_{EX} versus T_{EFF}/T_{MEM} there seemd
365 to be better correlation (Supp. Fig.5C).
366 These results are similar to previously published estimates in B cells, and has been
367 generally reported for eukaryotic cells[43, 44], and underscores the importance of performing
368 proteomic profiling for accurate characterization of the protein interactome of the cell, since
369 transcriptional profiling might not be the ideal proxy for protein abundance for all proteins and
370 under all conditions.
371

372 **Discussion**
373
374 We performed the first in vivo longitudinal proteomic profiling of antigen-specific CD8 T cell in
375 the context of both acute and chronic viral infection compared to naïve T cells. Our analyses
376 showed dynamic protein changes accompanying transitions between cell states in acute and
377 chronic infections that are in line with previously reported transcriptional and epigenetic studies[2,
378 8, 10, 24]. Most modulations of the T cell proteome occur at the early stages of infection following
379 activation, as the cells exit the naïve state, whereas subsequent modulations as the cell
380 differentiates during the intermediate and late stages of infection are more limited. Longitudinal
381 proteomic profiling during acute viral infection corroborated with previously published
382 transcriptional and epigenetic characterization of these cells, but several proteins identified by
383 our protein abundance were not previously investigated for their role in T cell differentiation in
384 the context of acute infection, and future studies are needed to investigate their potential role in
385 T cell differentiation. Using acute LCMV-Arm in parallel with LCMV-Cl13 enabled defining
386 common proteomic modules that suggests they represent a core proteomic program of T cell
387 differentiation, versus acute-specific and chronic-specific programs. Analysis of the LCMV-Cl13
388 chronic infection setting showed similar patterns for protein abundance of T_{EX}-associated
389 established markers that go in line with previously reported transcriptional and epigenetic
390 profiling in the same LCMV mouse model, as well as in other T cell exhaustion/dysfunction
391 models and datasets. More importantly, our protein abundance profiling of T_{EX} revealed novel
392 proteins with potential role in the exhaustion biology that necessitates investigation to validate
393 their specific function.
394
395 The fields of immunology and immunotherapy are on a quest for novel interventions to
396 enhance the efficacy and durability of immunotherapy. One overlooked and understudied
397 aspect for T cell biology is profiling the biochemical alterations within the cells, including the
398 protein interaction landscape that highlights pathways which may functionally influence the
399 exhausted state. Despite thorough characterization of T cell differentiation using microarray[10,
400 24], bulk RNAseq[5, 35], and single-cell RNAseq[45, 46], numerous studies highlighted the limited
401 correlation between RNA and protein levels, and the discordance between the half-lives of
402 mRNA and their corresponding proteins, underscoring the fact that transcriptional profiling is not
403 an ideal proxy for protein expression[12, 13]. Several endeavors were made to characterize
404 modulation of the protein-interactome of T cells upon activation in vitro, and the profiling of cells
405 from human samples ex-vivo, the direct *ex-vivo* mapping of the proteome associated with the
406 different states of T cell differentiation under various conditions is lacking. This data is essential
407 since it could bring invaluable insights into biochemical networks driving the T cell
408 effector/memory and exhaustion programs, as well as identify novel roles of specific proteins in
409 the differentiation of T cells that might have been overlooked due to discrepancies between the
410 gene expression levels measured by transcriptional profiling and the actual protein abundance
411 which could only be resolved by proteomic profiling. Future work should focus on dissecting the
412 specific role of newly reported proteins in our dataset in T cell differentiation, and their impact in
413 the modulation of the protein interactome of CD8 T cells.
414
415 State-of-the-art mass spectrometry-based proteomics is capable of quantifying
416 thousands of proteins[47], and is a powerful tool for studying both biochemical networks and
417 proteomic phenotypes. While proteomics has been applied to provide a better understanding of

418 T cell activation *in vitro* [15, 16, 17, 48], there is no systematic proteomic study investigating
419 differentiation of antigen-specific T cells directly *ex-vivo*. A global understanding of the
420 proteomic landscape accompanying T cell exhaustion will highlight opportunities for therapeutic
421 intervention. Defining the exhaustion-specific biochemical alterations and functional pathways
422 holds promise to identify novel targets for immunotherapeutic interventions that were not
423 identified by transcriptional profiling. Indeed, our preliminary analyses for applying protein
424 abundance profiling of T_{EX} using the well-established LCMV mouse model identified proteins
425 differentially abundant in T_{EX} compared to T cells in acute settings that were not previously
426 identified by other profiling methods. The work presented here is an endeavor to address
427 important unanswered questions: Which differentially abundant T_{EX}-associated proteins
428 functionally impact the exhaustion program? and what is the potential of manipulating these
429 exhaustion-associated proteins to synergize with checkpoint blockade?
430
431 Mass spectrometry-based proteomics is a powerful tool for studying the dynamics of
432 mRNA translation kinetics and protein turnover in T cells [49], or the systematic assessment of T
433 cell activation mediated by the T cell antigen receptor [50]. To date, there is no systematic
434 proteomic study investigation T cell exhaustion with antigen-specific cells in the LCMV model,
435 arguably the most well established and characterized model for studying T cell differentiation in
436 the context of acute and chronic infection[2, 7, 8, 9, 10, 24, 25, 26, 27]. To our knowledge, our application
437 of cutting-edge proteomics to study this well-established mouse model of T cell differentiation is
438 the first endeavor for an unbiased longitudinal proteomic analysis of antigen-specific exhausted
439 T cells directly *ex-vivo*. We have pioneered the use of proteomic analysis to study T cell
440 exhaustion in this model system, demonstrating striking results that recapitulate known
441 exhaustion markers and identify novel proteins of interest. Investigating the potential role of
442 these understudied proteins in the T_{EX}-biology could unravel promising drug targets.
443

Author contributions

MSA conceptualized the study. MSA and DEG conceived and designed the experiments. ASD and AO performed the immunology experiments with help from AF, SM, CN, AA, and CR. SM and CN provided technical help with flowcytometry panels. ASD was responsible for mouse breeding and colony maintenance with help from AAG. CMB performed the proteomics experiments with help from SLW. CMB performed the proteomic analyses. CMB performed the bioinformatic analyses. MSA wrote the manuscript. CMB prepared the figures with help from ASD and MSA.

Acknowledgements

This work was supported by Emory MP3 Seed Grant (00121861), and the Department of Pathology and Laboratory Medicine Start-up funds to MSA and DEG. CMB is the recipient of international Vetenskapsrådet postdoctoral fellowship.

The authors would like to thank members of Hakeem and Gordon labs, as well as members of PATRU and EVC for their valuable discussions and comments.

460 **Materials & Methods**
461
462 **Mice**
463 Age and sex matched C57BL/6 mice (CD45.2+) from The Jackson Laboratory between the ages
464 of 5-7 weeks, were used for all infection experiments. Both male and female mice were used in
465 the study. P14 TCR transgenic mice expressing a TCR specific for the H-2D^b GP33-41 epitope of
466 LCMV were bred at Emory University. Transgenic P14 CD8 T cells were harvested from mice
467 aged between 6-24 weeks from donor P14 mice matching the gender of the recipient mice. Mice
468 were maintained in a temperature-controlled animal facility at Emory University with a 12-h
469 light/dark cycle. All experimental procedures and breeding conditions were in accordance with
470 Institutional Animal Care and Use Committee (IACUC) guidelines for Emory University.
471
472 **Adoptive T cell transfer and LCMV infections**
473 Peripheral blood mononuclear cells (PBMCs) containing P14 CD8+ T cells (CD45.1$^+$) were
474 adoptively transferred intravenously (i.v.) into recipient mice (CD45.2$^+$) one day before infection
475 with LCMV. Recipient mice were engrafted with either 5×10^3 P14 cells for LCMV-Arm, and 1×10^3
476 P14 cells for LCMV-Cl13. For acute viral infections, mice were injected intraperitoneally (i.p) with
477 2×10^5 plaque-forming units (PFU) of LCMV-Arm. For chronic viral infections, mice were injected
478 i.v. with 4×10^6 PFU of LCMV-Cl13. LCMV-Arm and Cl13 were grown in BHK cells (ATCC, catalog
479 no. CCL-10) at a multiplicity of 0.01, 0.02 and/or 0.1 and supernatants were harvested at 60h
480 post-infection. Viral productions were titrated on VERO cells (ATCC, catalog no. CCL-81) using
481 plaque assay as previously described (1).
482
483 **Cell preparation**
484 Spleens isolated from mice at each time point (days 8, 15, and 30) post-infections with LCMV-
485 Arm and Cl13, were collected and homogenized together as a pooled sample using 70-µm cell
486 strainers to remove clumps. Cells were then centrifuged at 500x *g* for 5 minutes at 4°C. After
487 removing the supernatant, the cell pellet was resuspended in ammonium-chloride-potassium
488 (ACK) lysis buffer and incubated for 3 minutes at room temperature to lyse the red blood cells.
489 After incubation, an additional 20 mL of RPMI + 1% fetal bovine serum (FBS) was added to
490 neutralize the lysis buffer, and the cells were centrifuged at 500x *g* for 5 minutes at 4°C. The
491 resulting cell pellet was resuspended in RPMI + 10% FBS, and then counted. The splenocytes
492 were then used for flow cytometry and cell sorting. Before cell sorting, CD8+ T cells were enriched
493 from total splenocytes using the EasySep™ Mouse CD8+ T Cell Isolation Kit (STEMCELL
494 Technologies) (routinely >90% purity).
495
496 **Antibodies, flow cytometry and cell sorting**
497 The following fluorochrome-conjugated antibodies were used (clone mentioned in parentheses).
498 From Biolegend: anti-CD44–BV785 (IM7), dilution 1:300; anti-CD45.1–A700 (A20), 1:200; anti-
499 CD69–BV785 (H1.2F3), 1:200; anti-CD127–PE-Cy5 (A7R34), 1:200; anti-PD-1–PE-Cy7 (RMP1-
500 30), 1:200; anti-PD-1–APC-Fire 810 (29F.1A12), 1:200; anti-TIM3–BV605 (RMT3-23), 1:200;
501 anti-CX3CR1–BV650 (SA011F11), 1:200. From BD Biosciences: anti-CD8–BV650 (53–6.7),
502 1:200; anti-CD8–BUV805 (53–6.7), 1:200; anti-CD44–BUV737 (IM7), 1:200; anti-CD45.1–FITC
503 (A20), 1:200; anti-CD45.1–BUV496 (A20), 1:200; anti-CD39–BV711 (Y23-1185), 1:200; anti-PD-
504 1–BV786 (29F.1A12), 1:200; anti-Ly108–BB700 (13G3), 1:200; anti-granzyme–PE-CF594
505 (GB12), 1:100; anti-TCF-1/TCF7–R718 (S33-966), 1:100. From ThermoFisher Scientific: anti-

506 CD101–PE-Cy7 (Moushi101), 1:100; Live/Dead Fixable Aqua Dead Cell Stain Kit, 1:500;
507 Live/Dead Fixable Blue Dead Cell Stain Kit, 1:500. From Miltenyi Biotec: anti-TOX–APC
508 (REA473), 1:100. From Southern Biotech: anti-KLRG1–FITC (2F1), 1:150. Tetramers of MHC
509 class I H-2D^b GP33 were obtained from the NIH Tetramer Facility, Emory University, dilution
510 1:500.
511 Flow cytometry surface staining was performed by incubating cells with indicated antibodies for
512 20 minutes at 4°C. Intracellular staining was conducted with the eBioscience™
513 Foxp3/Transcription Factor Fixation/Permeabilization Kit (Thermo Fisher Scientific). Flow
514 cytometry data were obtained using BD FACSymphony™ A5 prior to sorting to examine the
515 phenotypes of LCMV-specific CD8 T cells. Subsequently, Cytek Aurora (Cytek Biosciences) was
516 used to achieve greater depth in phenotypic analysis. Data were analyzed using FlowJo™ v10.10
517 Software (FlowJo, LLC).
518 The enriched CD8+ T cells were stained on ice for 20 minutes with the relevant antibodies
519 cocktail. P14 cells (CD45.1$^+$GP33$^+$) were sorted with a FACS Aria II (BD Biosciences) using a 70-
520 mM nozzle in RPMI, 10% FBS. P14 cells were sorted from different time points on days 8, 15,
521 and 30 post-infections with LCMV in four replicate experiments. Naïve P14 cells were also sorted
522 to provide a benchmark for protein expression in naïve T cells. At least 2x10^5 antigen-specific
523 CD8 T cells were sorted from the different samples. Following FACS sorting, cells were washed
524 twice in ice-cold PBS and frozen pellets were used for proteomics analysis. Sorted cells were
525 washed twice in PBS and snap-frozen at -80 °C.
526
527 **Proteomics sample preparation**
528 Cell pellets were resuspended in 100 mM Tris pH 8, supplemented with 1% SDC, 10 mM TCEP,
529 and 40 mM CAA. Samples were boiled for 10 min at 95 °C and sonicated in a Bioruptor
530 (Diagenode) for 10 cycles of 30 sec on/30 sec off. The protein amount was determined by BCA
531 following manufacturer instructions (Thermo Fisher Scientific) and samples were digested
532 overnight with a 1:100 (w/w) Trypsin/Lys-C Mix (Promega) at 37 °C. 200 ng of peptides were
533 loaded onto preconditioned EvoTips (EvoSep) and washed following manufacturer instructions.
534
535 **LC-MS/MS**
536 Samples were injected in an EvoSep One system (EvoSep) coupled to a timsTOF Pro2 mass-
537 spectrometer (Bruker Daltonics). The peptides were loaded on a 15 cm Aurora Elite CSI column
538 (IonOpticks) and chromatographic separation was achieved using the predefined 20 SPD method.
539 The mass-spectrometer operated in positive polarity for data collection using data-independent
540 acquisition (diaPASEF) mode[51]. DIA isolation windows were optimized by py_diAID, consisting of
541 4 ion mobility windows and 12 mass isolation windows[52]. All spectra were acquired within an m/z
542 range of 100 to 1700 and fragmentation energy was set to 20 eV at 0.85 1/K0 and 59 eV at 1.30
543 1/K0.
544
545 **Proteomics data analysis**
546 Protein identification and quantification were performed using Spectronaut[53] (version 18) in
547 library-free mode using the Mus musculus SwissProt database (UP000000589, downloaded on
548 7.1.2022, 17'090 entries) with default settings. Modifications were defined as follows,
549 Carbamidomethylation (C) as a fixed modification, and Acetyl (Protein N-term) and Oxidation (M)
550 as variable modifications. All further data processing was performed in R (version 4.3.1). Only
551 proteins with at least 3 quantified values in at least one sample group were kept. Intensities were

552 normalized by median centering and logs2-scaling. Missing values were imputed by Bayesian
553 PCA imputation[54] and downshift sampling, for proteins missing at random or not at random,
554 respectively[55]. All statistical comparisons between the two groups were performed based on two-
555 tailed Student's t-tests. For analysis across multiple groups, ANOVA was employed. Gene
556 ontology enrichment analysis was performed in Metascape, defining all identified proteins as
557 background[56]. Correlations are reported as Pearson correlation unless otherwise noted. A p-value
558 below 0.05 was considered statistically significant.
559
560 **Integration of RNA sequencing data set**
561 Public Microarray data from *Doering et al.* was downloaded from the original publication and the
562 Gene Omnibus website[24]. Single-cell transcriptomics (scRNASeq) data from mouse TILs were
563 downloaded from *Andreatta et al*[57]. Correlation of scRNAseq data was performed with CS-CORE,
564 using default settings[58]. To increase the robustness of the correlation approach, only gene
565 products with an average read count of at least 0.2 in one of the cellular subsets, as defined in
566 the original publication, were considered.

567 **Data availability**
568 The mass spectrometry proteomics data files will be deposited to the ProteomeXchange
569 Consortium via the PRIDE partner repository[59].

570
571

572 **Figure legends**
573
574 **Figure 1: Longitudinal proteomic profiling of antigen-specific CD8 T highlighting the**
575 **differential expression of proteins in acute versus chronic conditions.** (**A**) Experimental
576 strategy detailing the profiling proteome-wide alteration in CD8+ T cell differentiating in acute
577 resolving and chronic viral infections. (**B, C**) Representative flow cytometry dot plots
578 demonstrating the levels of the canonical exhaustion marker PD-1 and the antigen-experienced
579 marker Klrg1. (**D**) Comparison of protein expression assessed through flow cytometry (top) and
580 proteomics (bottom). The absence of a measurement bar indicates no quantification. (**E**) Principal
581 component analysis (PCA) across all proteomics samples. (**F**) Quantification of protein
582 abundance alterations across the T cell differential axis in acute resolving and chronic viral
583 infections. Dark wedges represent up-regulated proteins ($p < 0.05$ from one-sided ANOVA,
584 log2FC > 1), while grey wedges signify down-regulated proteins ($p < 0.05$ from one-sided ANOVA,
585 log2FC > 1). N = 4 for all proteomics samples, with error bars representing mean ± standard
586 deviation.
587
588 **Figure 2: Expression profiles of proteins defining T cell activation and differentiation in the**
589 **context of acute LCMV-Arm infection.** (**A**) Unsupervised hierarchical clustering of proteins that
590 exhibit significant regulation ($p < 0.05$ from one-sided ANOVA) and log2FC > 1 along the T cell
591 differentiation pathway from naïve to the memory cell. (**B**) Longitudinal protein changes for
592 proteins within selected clusters. (**C**) Gene ontology enrichment analysis of selected protein
593 clusters derived from the heatmap. (**D, E, F**) Statistical analysis of protein alterations observed
594 from naïve to memory effector antigen-specific T cells. (**G**, **H, I**) Comparison between proteomics
595 measurements and data from a published microarray study by *Doering et al*.[24] N = 4 for all
596 proteomics samples and microarray samples.
597
598 **Figure 3: Common and distinct dynamic changes of the T cell proteome in the context of**
599 **acute LCMV-Arm and chronic LCMV-Cl13 infections.** (**A**) Unsupervised hierarchical
600 clustering of proteins that shows significant regulation ($p < 0.05$ from one-sided ANOVA) and
601 log2FC > 1 comparing acute resolving and chronic viral infections. (**B**) Comparison of protein
602 alterations between acute and chronic T cells across each clustering. (**C**) Distribution of protein
603 expression change belonging to the respiratory chain complex 1 across all samples. (**D**, **E**, **F**)
604 Scatter plots comparing protein expression changes of acute and chronic infected T cells
605 relative to Naïve ones on days 8, 15, and 30. (**G**) Volcano plot depicting proteins having
606 statistically significant abundance in CD8 T cells isolated from mice infected with Armstrong or
607 Clone 13 strains 30 days post-infection. (**H**) Protein signatures of statically regulated proteins
608 from G), extracted by CellMarker. N = 4 for all proteomics samples. Sample correlation was
609 determined using Pearson correlation. The Jaccard index was employed to compare statically
610 significant regulated proteins ($p < 0.05$, absolute log2 FC > 1).
611
612 **Figure 4: Integration of T cell mRNA and protein profiling reveals variable correlation**
613 **profiles for different proteins.** (**A**) Scatter plots comparing proteomics data with microarray
614 data from *Doering et al*. for the various time points. (**B**) Evaluation of microarray depth concerning
615 significantly regulated proteins identified by either microarray or proteomics experiments. Sample
616 correlation was determined using Pearson correlation.

617 **Supplementary Figure legends**
618
619 **Supplementary Figure 1: Flowcytometry validation of the phenotype and sorting purity of**
620 **antigen-specific CD8 T cells used for proteomic profiling by MassSpec.**
621 (**A**) Gating strategy for flow cytometry analysis.
622 (**B**) Representative dot plots of the phenotypic analysis of antigen-specific CD8 T cells.
623 (**C**) Representative dot plots reflecting the sorting purity (post-sorting, right panels) compared to
624 the original frequencies pre-sorting.
625
626 **Supplementary Figure 2: Logistics of protein abundance profiling of antigen-specific CD8**
627 **T cells in the context of acute and chronic infection.**
628 (**A**) Number of quantified proteins in the different samples.
629 (**B**) Correlation between the different samples from the four replicates .
630 (**C-E**) Dynamic range for the protein abundance quantification for the naïve (**C**), acute (**D**), and
631 chronic (**E**) samples.
632 (**F**) Comparison of protein expression assessed through flow cytometry (top) and proteomics
633 (bottom). The absence of a measurement bar indicates no quantification. **E**) Principal
634 component analysis (PCA) across all proteomics samples.
635 (**G**) Correlation between protein expression levels assessed through flow cytometry (Y-axis) and
636 proteomics (X-axis).
637
638 **Supplementary Figure S3: Protein abundance alterations during T cell differential in acute**
639 **viral infection.**
640 (**A**) Quantification of protein abundance alterations across the T cell differential axis in acute viral
641 infection.
642 (**B**) Significant protein alterations intersections at the different time points post-infection with
643 acute LCMV-Arm compared to naïve CD8 T cells.
644
645 **Supplementary Figure S4: Protein alterations in the context of T cell exhaustion**
646 (**A**) Quantification of protein abundance alterations at the specific time points between the acute
647 and chronic infections at a given time point.
648 (**B**) Biological processes associated with significant protein alterations intersections at the
649 different time points post-infection with acute LCMV-Arm compared to naïve CD8 T cells.
650 (**C-D**) Volcano plots depicting proteins having statistically significant abundance in CD8 T cells
651 isolated from mice infected with Armstrong or Clone 13 strains at 8 (**C**) or 15 (**D**) days post-
652 infection.
653 (**E**) Distribution of protein expression change belonging to the mitochondrial proteins across all
654 samples.
655
656 **Supplementary Figure S5: Integration of transcriptional and proteomic profiling of**
657 **antigen-specific CD8 T cells.**
658 (**A**) Comparison of median microarray count and median log2 protein intensity across samples.
659 (**B**) Correlation between the log2 fold change of proteins (X-axis) versus log2 fold change of
660 mRNA (Y-axis) in Cl13 samples compared to Arm samples.
661 (**C**) Heatmaps reflecting dynamic changes in selected exhaustion-associated markers across
662 samples, from proteomic analysis (left) and microarray analysis (right).
663 Microarray data from *Doering et al*.[24]
664
665

References

1. Kaech, S.M. & Cui, W. Transcriptional control of effector and memory CD8+ T cell differentiation. *Nat Rev Immunol* **12**, 749-761 (2012).

2. Scott-Browne, J.P. *et al.* Dynamic Changes in Chromatin Accessibility Occur in CD8(+) T Cells Responding to Viral Infection. *Immunity* **45**, 1327-1340 (2016).

3. Kaech, S.M. *et al.* Selective expression of the interleukin 7 receptor identifies effector CD8 T cells that give rise to long-lived memory cells. *Nat Immunol* **4**, 1191-1198 (2003).

4. Joshi, N.S. *et al.* Inflammation directs memory precursor and short-lived effector CD8(+) T cell fates via the graded expression of T-bet transcription factor. *Immunity* **27**, 281-295 (2007).

5. Hudson, W.H. *et al.* Expression of novel long noncoding RNAs defines virus-specific effector and memory CD8(+) T cells. *Nat Commun* **10**, 196 (2019).

6. McLane, L.M., Abdel-Hakeem, M.S. & Wherry, E.J. CD8 T Cell Exhaustion During Chronic Viral Infection and Cancer. *Annu Rev Immunol* **37**, 457-495 (2019).

7. Blackburn, S.D. *et al.* Coregulation of CD8+ T cell exhaustion by multiple inhibitory receptors during chronic viral infection. *Nat Immunol* **10**, 29-37 (2009).

8. Ghoneim, H.E. *et al.* De Novo Epigenetic Programs Inhibit PD-1 Blockade-Mediated T Cell Rejuvenation. *Cell* **170**, 142-157 e119 (2017).

9. Pauken, K.E. *et al.* Epigenetic stability of exhausted T cells limits durability of reinvigoration by PD-1 blockade. *Science* **354**, 1160-1165 (2016).

10. Wherry, E.J. *et al.* Molecular signature of CD8+ T cell exhaustion during chronic viral infection. *Immunity* **27**, 670-684 (2007).

11. Wherry, E.J. & Kurachi, M. Molecular and cellular insights into T cell exhaustion. *Nat Rev Immunol* **15**, 486-499 (2015).

12. Wang, D. *et al.* A deep proteome and transcriptome abundance atlas of 29 healthy human tissues. *Mol Syst Biol* **15**, e8503 (2019).

13. Edfors, F. *et al.* Gene-specific correlation of RNA and protein levels in human cells and tissues. *Mol Syst Biol* **12**, 883 (2016).

14. Damasio, M.P. *et al.* Extracellular signal-regulated kinase (ERK) pathway control of CD8+ T cell differentiation. *Biochem J* **478**, 79-98 (2021).

15. Howden, A.J.M. *et al.* Quantitative analysis of T cell proteomes and environmental sensors during T cell differentiation. *Nat Immunol* **20**, 1542-1554 (2019).

16. Hukelmann, J.L. *et al.* The cytotoxic T cell proteome and its shaping by the kinase mTOR. *Nat Immunol* **17**, 104-112 (2016).

17. Marchingo, J.M., Sinclair, L.V., Howden, A.J. & Cantrell, D.A. Quantitative analysis of how Myc controls T cell proteomes and metabolic pathways during T cell activation. *Elife* **9** (2020).

18. Ross, S.H., Rollings, C.M. & Cantrell, D.A. Quantitative Analyses Reveal How Hypoxia Reconfigures the Proteome of Primary Cytotoxic T Lymphocytes. *Front Immunol* **12**, 712402 (2021).

19. Rieckmann, J.C. *et al.* Social network architecture of human immune cells unveiled by quantitative proteomics. *Nat Immunol* **18**, 583-593 (2017).

20. Wolf, T. *et al.* Dynamics in protein translation sustaining T cell preparedness. *Nat Immunol* **21**, 927-937 (2020).

21. Joshi, R.N. *et al.* TcellSubC: An Atlas of the Subcellular Proteome of Human T Cells. *Front Immunol* **10**, 2708 (2019).

22. Canale, F.P. *et al.* Proteomics of immune cells from liver tumors reveals immunotherapy targets. *Cell Genom* **3**, 100331 (2023).

23. Jiang, Y. *et al.* Proteomics identifies new therapeutic targets of early-stage hepatocellular carcinoma. *Nature* **567**, 257-261 (2019).

24. Doering, T.A. *et al.* Network analysis reveals centrally connected genes and pathways involved in CD8+ T cell exhaustion versus memory. *Immunity* **37**, 1130-1144 (2012).

25. Fuller, M.J. & Zajac, A.J. Ablation of CD8 and CD4 T cell responses by high viral loads. *J Immunol* **170**, 477-486 (2003).

26. Wherry, E.J., Blattman, J.N., Murali-Krishna, K., van der Most, R. & Ahmed, R. Viral persistence alters CD8 T-cell immunodominance and tissue distribution and results in distinct stages of functional impairment. *J Virol* **77**, 4911-4927 (2003).

27. Zajac, A.J. *et al.* Viral immune evasion due to persistence of activated T cells without effector function. *J Exp Med* **188**, 2205-2213 (1998).

28. Sen, D.R. *et al.* The epigenetic landscape of T cell exhaustion. *Science* **354**, 1165-1169 (2016).

29. Bengsch, B. *et al.* Bioenergetic Insufficiencies Due to Metabolic Alterations Regulated by the Inhibitory Receptor PD-1 Are an Early Driver of CD8(+) T Cell Exhaustion. *Immunity* **45**, 358-373 (2016).

30. Scott-Browne, J.P. *et al.* Dynamic Changes in Chromatin Accessibility Occur in CD8+ T Cells Responding to Viral Infection. *Immunity* **45**, 1327-1340 (2016).

31. Paley, M.A. *et al.* Progenitor and terminal subsets of CD8+ T cells cooperate to contain chronic viral infection. *Science* **338**, 1220-1225 (2012).

32. Shin, H. *et al.* A role for the transcriptional repressor Blimp-1 in CD8(+) T cell exhaustion during chronic viral infection. *Immunity* **31**, 309-320 (2009).

33. Alfei, F. *et al.* TOX reinforces the phenotype and longevity of exhausted T cells in chronic viral infection. *Nature* **571**, 265-269 (2019).

34. Khan, O. *et al.* TOX transcriptionally and epigenetically programs CD8(+) T cell exhaustion. *Nature* **571**, 211-218 (2019).

35. Scott, A.C. *et al.* TOX is a critical regulator of tumour-specific T cell differentiation. *Nature* **571**, 270-274 (2019).

36. Yao, C. *et al.* Single-cell RNA-seq reveals TOX as a key regulator of CD8(+) T cell persistence in chronic infection. *Nat Immunol* **20**, 890-901 (2019).

37. Sharma, P. & Allison, J.P. The future of immune checkpoint therapy. *Science* **348**, 56-61 (2015).

38. Ribas, A. & Wolchok, J.D. Cancer immunotherapy using checkpoint blockade. *Science* **359**, 1350-1355 (2018).

39. Abdel-Hakeem, M.S. *et al.* Epigenetic scarring of exhausted T cells hinders memory differentiation upon eliminating chronic antigenic stimulation. *Nat Immunol* **22**, 1008-1019 (2021).

40. Yates, K.B. *et al.* Epigenetic scars of CD8(+) T cell exhaustion persist after cure of chronic infection in humans. *Nat Immunol* **22**, 1020-1029 (2021).

41. Nicolet, B.P. & Wolkers, M.C. The relationship of mRNA with protein expression in CD8+ T cells associates with gene class and gene characteristics. *PLoS One* **17**, e0276294 (2022).

42. Tan, H. *et al.* Integrative Proteomics and Phosphoproteomics Profiling Reveals Dynamic Signaling Networks and Bioenergetics Pathways Underlying T Cell Activation. *Immunity* **46**, 488-503 (2017).

43. Salerno, F. *et al.* An integrated proteome and transcriptome of B cell maturation defines poised activation states of transitional and mature B cells. *Nat Commun* **14**, 5116 (2023).

44. Vogel, C. & Marcotte, E.M. Insights into the regulation of protein abundance from proteomic and transcriptomic analyses. *Nat Rev Genet* **13**, 227-232 (2012).

45. Daniel, B. *et al.* Divergent clonal differentiation trajectories of T cell exhaustion. *Nat Immunol* **23**, 1614-1627 (2022).

46. Giles, J.R. *et al.* Shared and distinct biological circuits in effector, memory and exhausted CD8(+) T cells revealed by temporal single-cell transcriptomics and epigenetics. *Nat Immunol* **23**, 1600-1613 (2022).

47. Demichev, V. *et al.* dia-PASEF data analysis using FragPipe and DIA-NN for deep proteomics of low sample amounts. *Nature Communications* **13**, 3944 (2022).

48. Ross, S.H. *et al.* Phosphoproteomic Analyses of Interleukin 2 Signaling Reveal Integrated JAK Kinase-Dependent and -Independent Networks in CD8(+) T Cells. *Immunity* **45**, 685-700 (2016).

49. Wolf, T. *et al.* Dynamics in protein translation sustaining T cell preparedness. *Nature Immunology 2020 21:8* **21**, 927-937 (2020).

50. Roncagalli, R. *et al.* Quantitative proteomics analysis of signalosome dynamics in primary T cells identifies the surface receptor CD6 as a Lat adaptor–independent TCR signaling hub. *Nature Immunology* **15**, 384-392 (2014).

51. Meier, F. *et al.* diaPASEF: parallel accumulation-serial fragmentation combined with data-independent acquisition. *Nat Methods* **17**, 1229-1236 (2020).

52. Skowronek, P. *et al.* Rapid and In-Depth Coverage of the (Phospho-)Proteome With Deep Libraries and Optimal Window Design for dia-PASEF. *Mol Cell Proteomics* **21**, 100279 (2022).

53. Bruderer, R. *et al.* Optimization of Experimental Parameters in Data-Independent Mass Spectrometry Significantly Increases Depth and Reproducibility of Results. *Mol Cell Proteomics* **16**, 2296-2309 (2017).

54. Jin, L. *et al.* A comparative study of evaluating missing value imputation methods in label-free proteomics. *Sci Rep* **11**, 1760 (2021).

55. Lazar, C., Gatto, L., Ferro, M., Bruley, C. & Burger, T. Accounting for the Multiple Natures of Missing Values in Label-Free Quantitative Proteomics Data Sets to Compare Imputation Strategies. *J Proteome Res* **15**, 1116-1125 (2016).

853 56. Zhou, Y. *et al.* Metascape provides a biologist-oriented resource for the analysis
854 of systems-level datasets. *Nat Commun* **10**, 1523 (2019).
855
856 57. Andreatta, M. *et al.* Interpretation of T cell states from single-cell transcriptomics
857 data using reference atlases. *Nat Commun* **12**, 2965 (2021).
858
859 58. Su, C. *et al.* Cell-type-specific co-expression inference from single cell RNA-
860 sequencing data. *Nat Commun* **14**, 4846 (2023).
861
862 59. Vizcaino, J.A. *et al.* ProteomeXchange provides globally coordinated proteomics
863 data submission and dissemination. *Nat Biotechnol* **32**, 223-226 (2014).
864
865

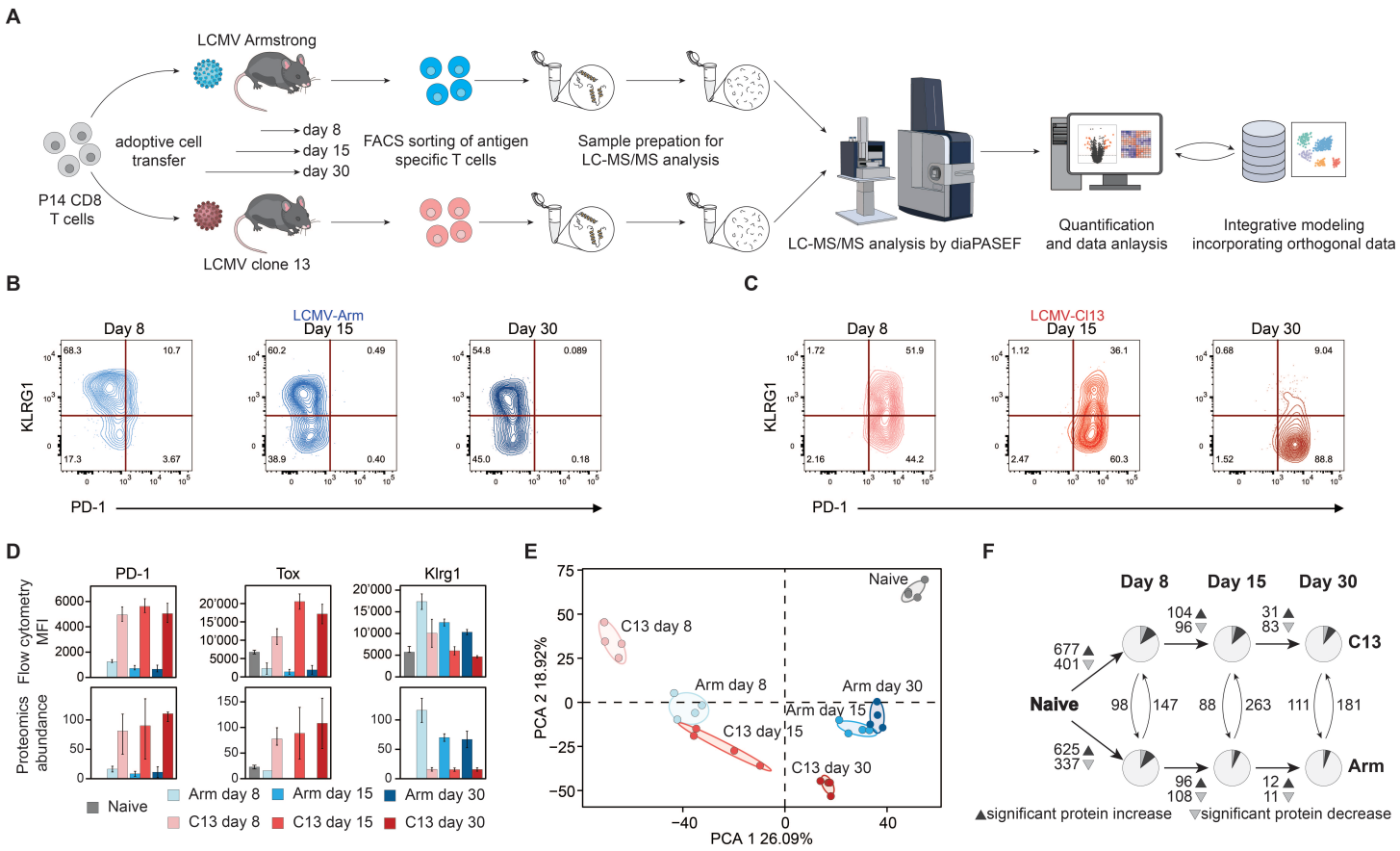

Figure 1: Longitudinal proteomic profiling of antigen-specific CD8 T highlighting the differential expression of proteins in acute versus chronic conditions. (**A**) Experimental strategy detailing the profiling proteome-wide alteration in CD8+ T cell differentiating in acute resolving and chronic viral infections. (**B, C**) Representative flow cytometry dot plots demonstrating the levels of the canonical exhaustion marker PD-1 and the antigen-experienced marker Klrg1. (**D**) Comparison of protein expression assessed through flow cytometry (top) and proteomics (bottom). The absence of a measurement bar indicates no quantification. (**E**) Principal component analysis (PCA) across all proteomics samples. (**F**) Quantification of protein abundance alterations across the T cell differential axis in acute resolving and chronic viral infections. Dark wedges represent up-regulated proteins ($p < 0.05$ from one-sided ANOVA, log2FC > 1), while grey wedges signify down-regulated proteins ($p < 0.05$ from one-sided ANOVA, log2FC > 1). N = 4 for all proteomics samples, with error bars representing mean ± standard deviation.

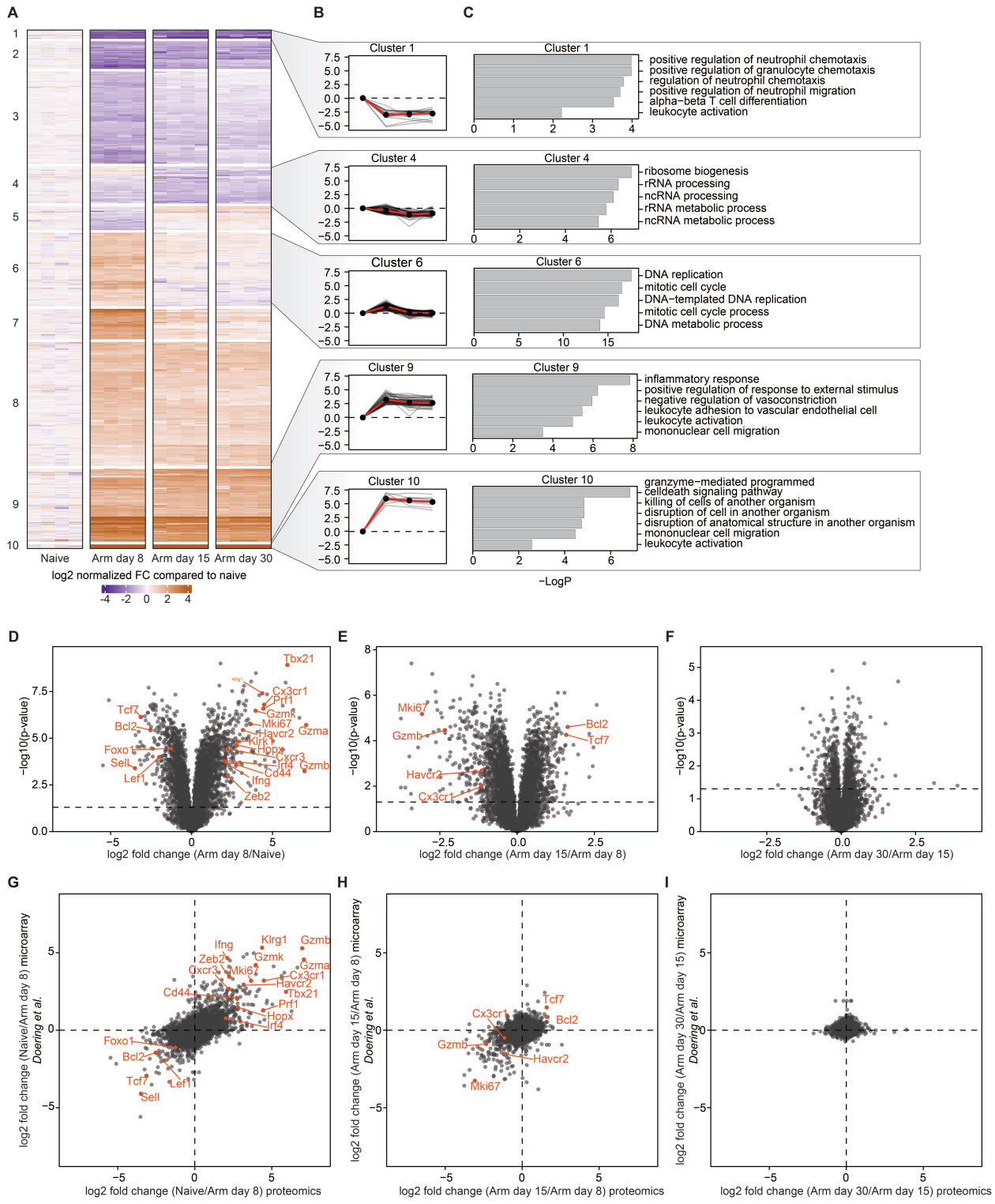

Figure 2: Expression profiles of proteins defining T cell activation and differentiation in the context of acute LCMV-Arm infection. (**A**) Unsupervised hierarchical clustering of proteins that exhibit significant regulation ($p < 0.05$ from one-sided ANOVA) and log2FC > 1 along the T cell differentiation pathway from naïve to the memory cell. (**B**) Longitudinal protein changes for proteins within selected clusters. (**C**) Gene ontology enrichment analysis of selected protein clusters derived from the heatmap. (**D, E, F**) Statistical analysis of protein alterations observed from naïve to memory effector antigen-specific T cells. (**G**, **H, I**) Comparison between proteomics measurements and data from a published microarray study by *Doering et al.*[24] N = 4 for all proteomics samples and microarray samples.

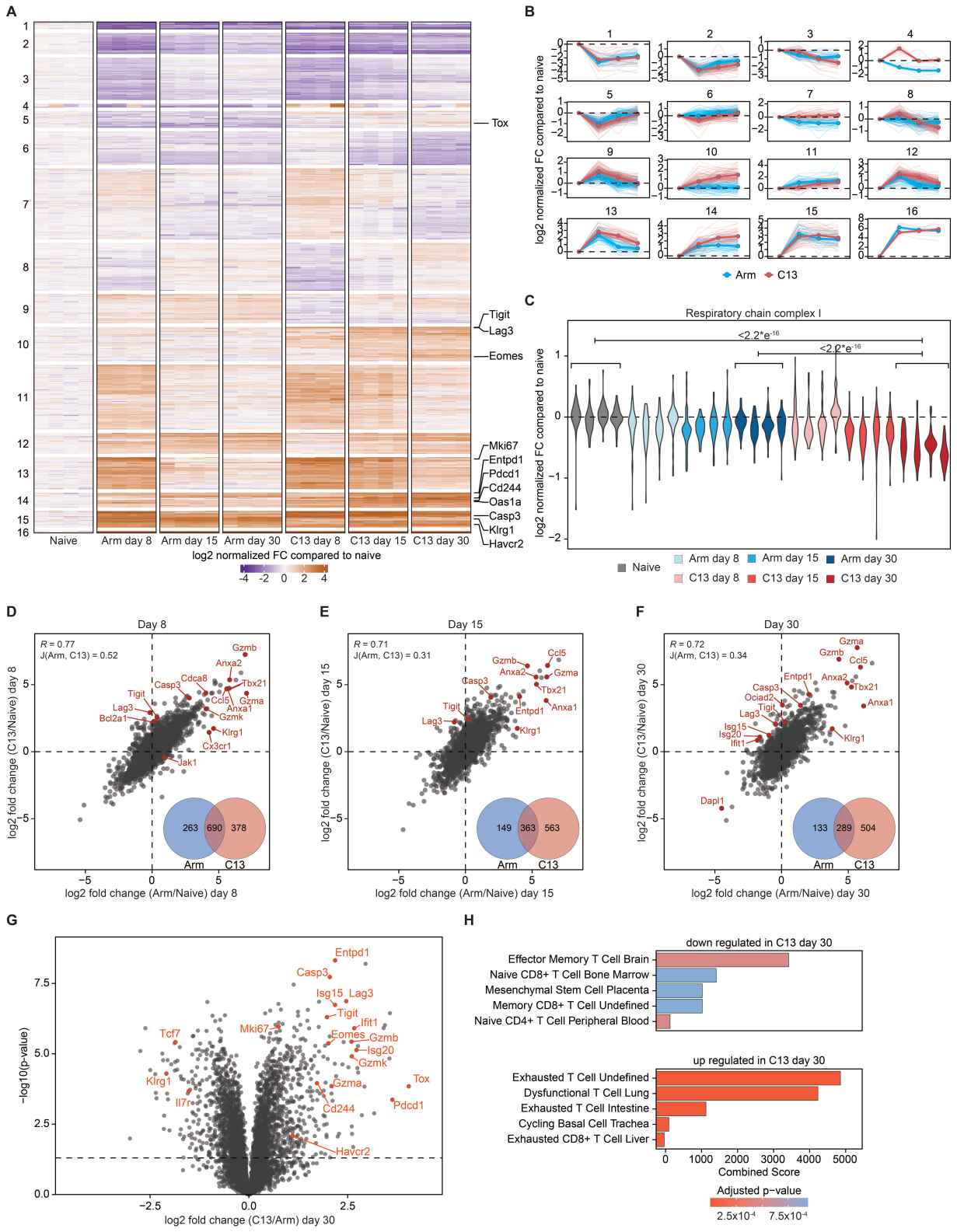

Figure 3: Common and distinct dynamic changes of the T cell proteome in the context of acute LCMV-Arm and chronic LCMV-Cl13 infections. (**A**) Unsupervised hierarchical clustering of proteins that shows significant regulation ($p < 0.05$ from one-sided ANOVA) and log2FC > 1 comparing acute resolving and chronic viral infections. (**B**) Comparison of protein alterations between acute and chronic T cells across each clustering. (**C**) Distribution of protein expression change belonging to the respiratory chain complex 1 across all samples. (**D**, **E**, **F**) Scatter plots comparing protein expression changes of acute and chronic infected T cells relative to Naïve ones on days 8, 15, and 30. (**G**) Volcano plot depicting proteins having statistically

significant abundance in CD8 T cells isolated from mice infected with Armstrong or Clone 13 strains 30 days post-infection. (**H**) Protein signatures of statically regulated proteins from G), extracted by CellMarker. N = 4 for all proteomics samples. Sample correlation was determined using Pearson correlation. The Jaccard index was employed to compare statically significant regulated proteins ($p < 0.05$, absolute log2 FC > 1).

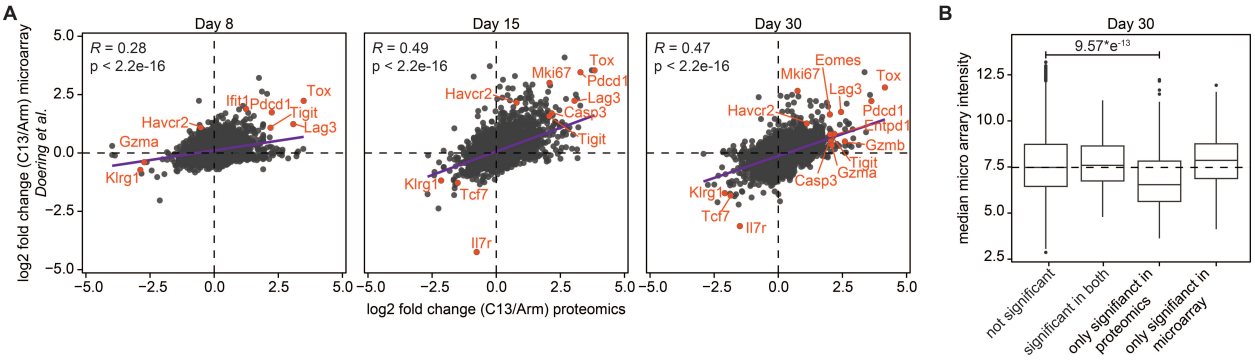

Figure 4: Integration of T cell mRNA and protein profiling reveals variable correlation profiles for different proteins. (**A**) Scatter plots comparing proteomics data with microarray data from *Doering et al*. for the various time points. (**B**) Evaluation of microarray depth concerning significantly regulated proteins identified by either microarray or proteomics experiments. Sample correlation was determined using Pearson correlation.

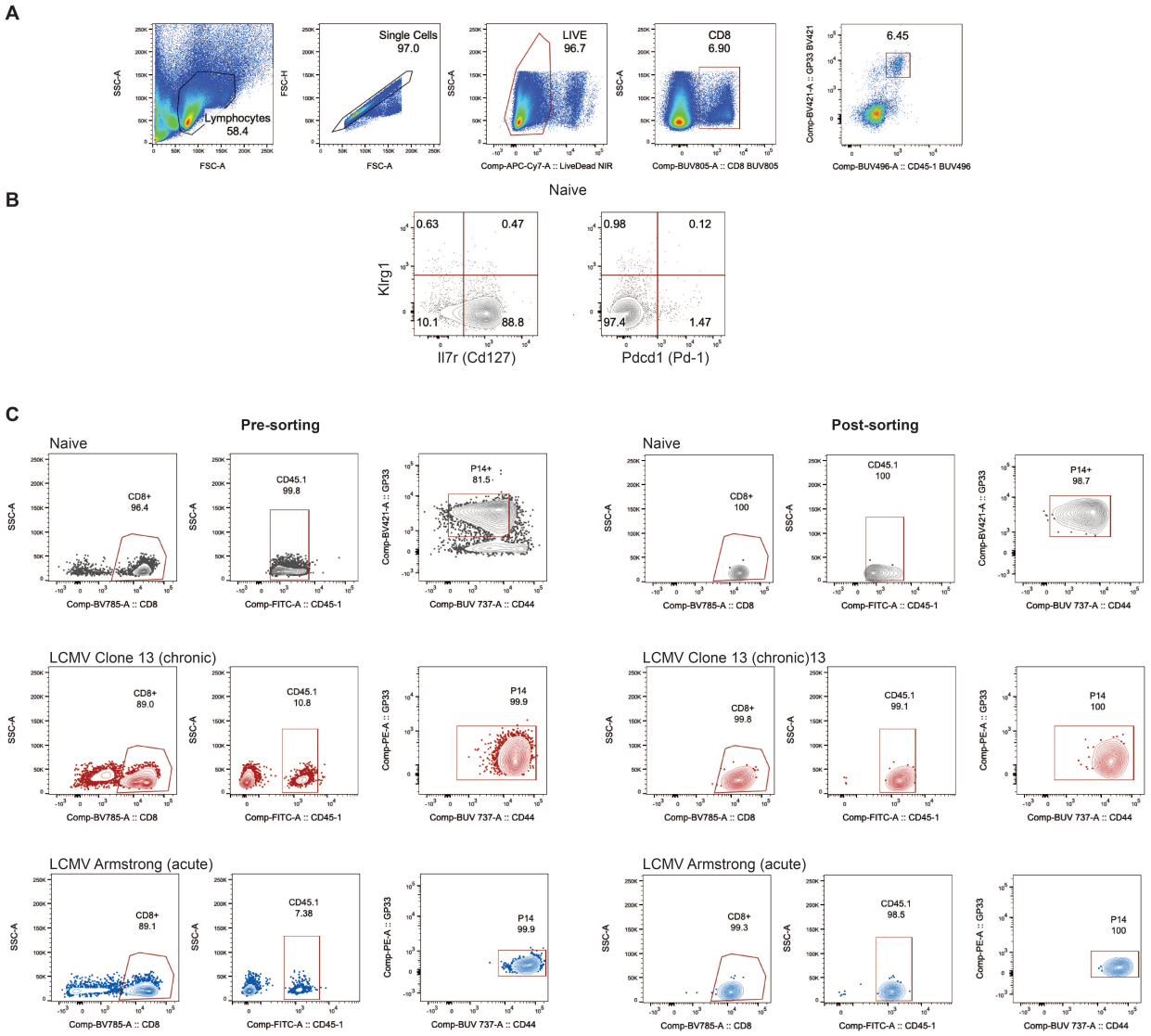

Supplementary Figure 1: Flowcytometry validation of the phenotype and sorting purity of antigen-specific CD8 T cells used for proteomic profiling by MassSpec. (**A**) Gating strategy for flow cytometry analysis. (**B**) Representative dot plots of the phenotypic analysis of antigen-specific CD8 T cells. (**C**) Representative dot plots reflecting the sorting purity (post-sorting, right panels) compared to the original frequencies pre-sorting.

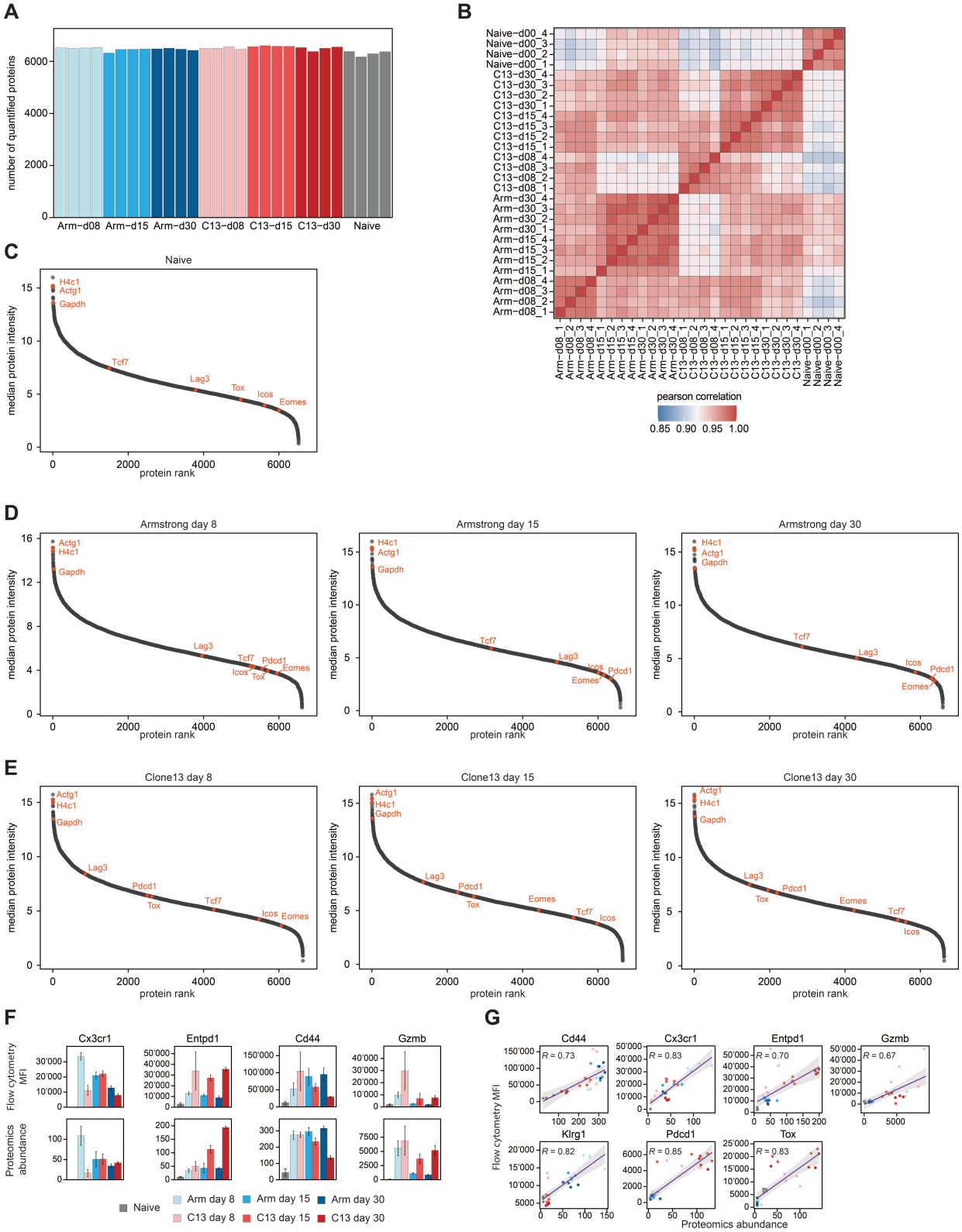

Supplementary Figure 2: Logistics of protein abundance profiling of antigen-specific CD8 T cells in the context of acute and chronic infection. (**A**) Number of quantified proteins in the different samples. (**B**) Correlation between the different samples from the four replicates . (**C-E**) Dynamic range for the protein abundance quantification for the naïve (**C**), acute (**D**), and chronic (**E**) samples. (**F**) Comparison of protein expression assessed through flow cytometry (top) and proteomics (bottom). The absence of a measurement bar indicates no quantification. (**E**) Principal component analysis (PCA) across all proteomics samples. (**G**) Correlation between protein expression levels assessed through flow cytometry (Y-axis) and proteomics (X-axis).

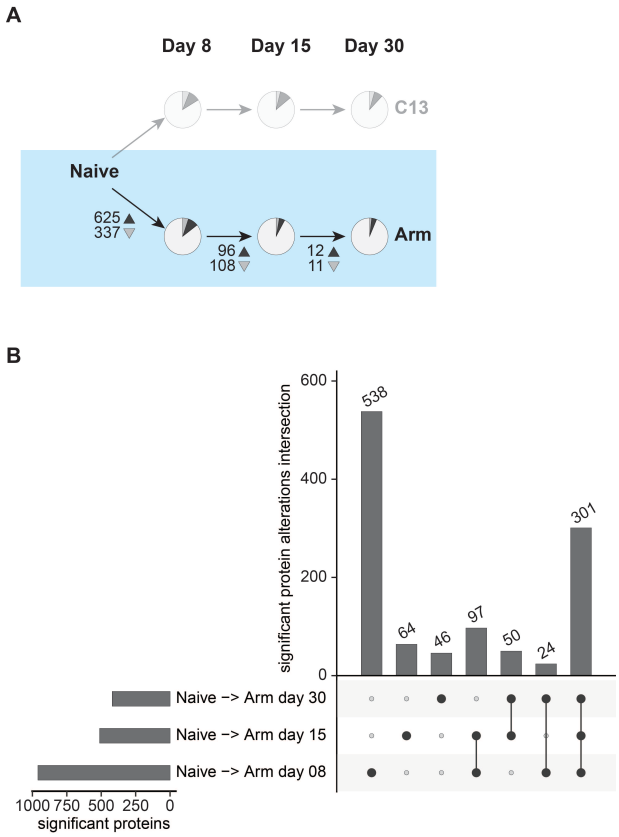

Supplementary Figure S3: Protein abundance alterations during T cell differential in acute viral infection. (**A**) Quantification of protein abundance alterations across the T cell differential axis in acute viral infection. (**B**) Significant protein alterations intersections at the different time points post-infection with acute LCMV-Arm compared to naïve CD8 T cells.

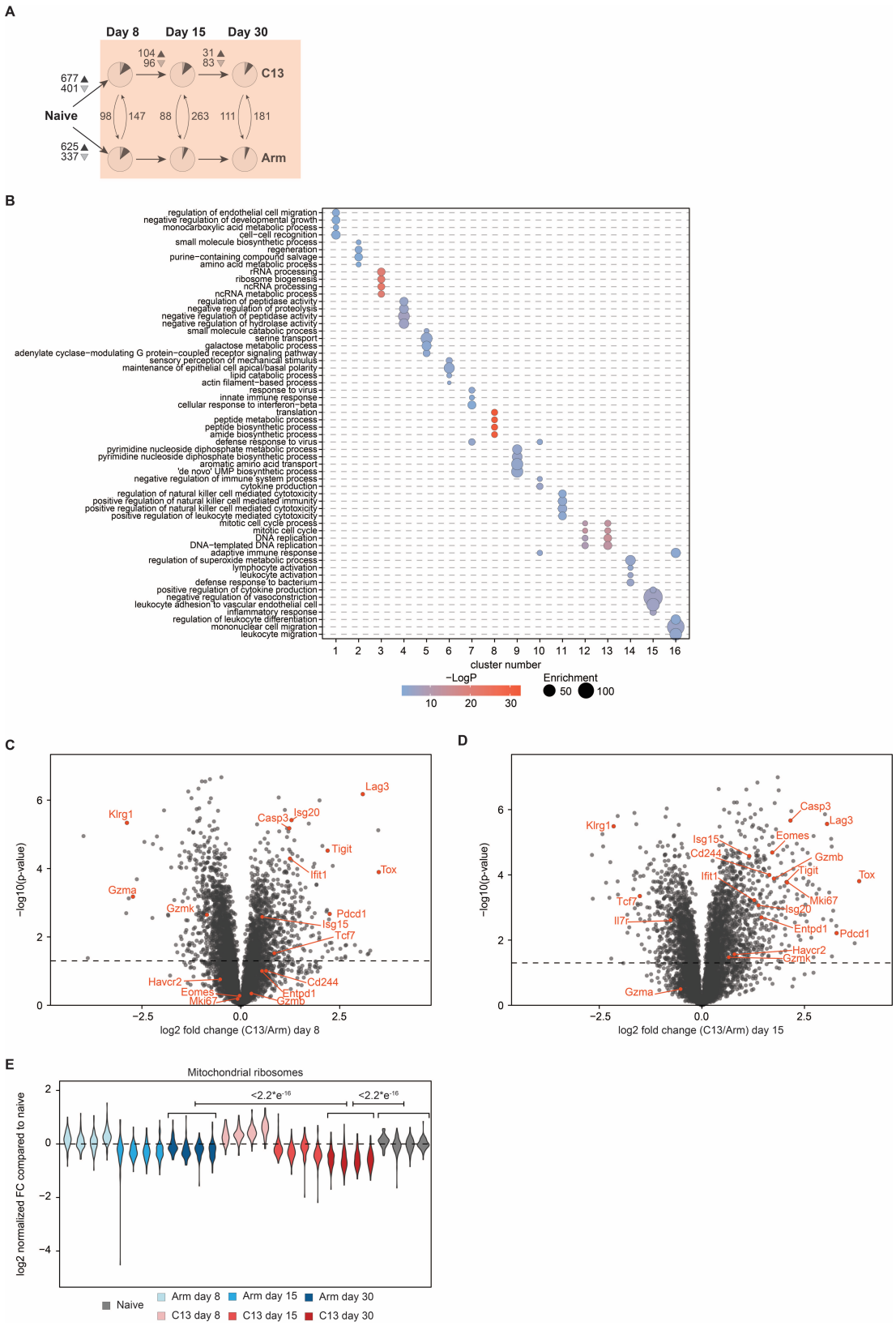

Supplementary Figure S4: Protein alterations in the context of T cell exhaustion. (**A**) Quantification of protein abundance alterations at the specific time points between the acute and chronic infections at a given time point. (**B**) Biological processes associated with significant protein alterations intersections at the different time points post-infection with acute LCMV-Arm compared to naïve CD8 T cells. (**C-D**) Volcano plots depicting proteins having statistically significant abundance in CD8 T cells isolated from mice infected with Armstrong or Clone 13 strains at 8 (**C**) or 15 (**D**) days post-infection. (**E**) Distribution of protein expression change belonging to the mitochondrial proteins across all samples.

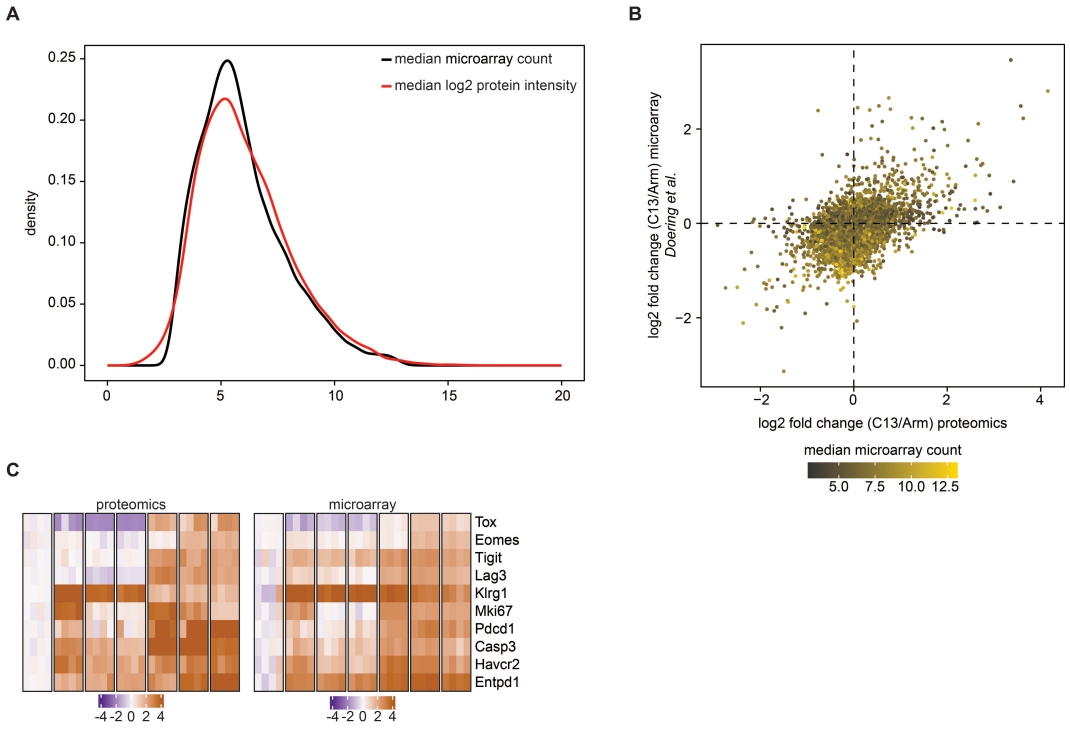

Supplementary Figure S5: Integration of transcriptional and proteomic profiling of antigen-specific CD8 T cells. (**A**) Comparison of median microarray count and median log2 protein intensity across samples. (**B**) Correlation between the log2 fold change of proteins (X-axis) versus log2 fold change of mRNA (Y-axis) in Cl13 samples compared to Arm samples. (**C**) Heatmaps reflecting dynamic changes in selected exhaustion-associated markers across samples, from proteomic analysis (left) and microarray analysis (right). Microarray data from *Doering et al*.[24].